Swiss J Geosci (2014) 107:81–99
DOI 10.1007/s00015-014-0159-7

P–T conditions of metabasites within regional metapelites in far-eastern Nepal Himalaya and its tectonic meaning

Takeshi Imayama

Received: 20 July 2013 / Accepted: 29 April 2014 / Published online: 22 May 2014

Abstract Metabasites exposed in far-eastern Nepal provide an important insight into the metamorphic evolution of the Himalayan orogen independent from data obtained on metapelites. The P–T conditions and formation process of mafic granulite intercalated within Early Oligocene migmatites and two amphibolites surrounded by Early Miocene metapelites were inferred from pseudosection modeling and conventional geothermobarometry combined with the occurrences of field and microstructures. A mafic granulite in the Higher Himalaya Crystalline Sequence (HHCS) yields P–T conditions of 6.5–8 kbar, 730–750 °C. The similar peak P–T condition and retrograde path with low P/T gradient of mafic granulite and surrounding migmatite indicate that both rocks were simultaneously metamorphosed and exhumed together along the tectonic discontinuities in the HHCS. In contrast, the P–T conditions (2–5 kbar, 500–600 °C) of highly-deformed amphibolite block above the Main Central Thrust (MCT) records significantly lower pressure than garnet-mica gneisses in the country rock, suggesting that the amphibolite block derived from upper unit of the MCT zone and became tectonically mixed with the gneisses of hanging wall near the surface. An amphibolite lense below the MCT preserves the prograde P–T conditions (6–7.5 kbar, 550–590 °C) of Early Miocene syn-tectonic metamorphism that occurred in the MCT zone. This study indicates the top-to-the south movement of the MCT zone results in the tectonic assembly of rocks with different P–T–t conditions near the MCT.

Keywords Nepal Himalaya · P–T evolution · Metabasites · Tectonic block

1 Introduction

The Himalaya is one of the best-documented examples of a continent–continent collision orogen containing an inverted metamorphic sequences characterized by peak metamorphic temperatures that progressively increases towards the upper structural levels (e.g. Le Fort 1975; Hodges 2000). The Higher Himalaya Crystalline Sequence (HHCS) consisting of high grade rocks is bounded by the Main Central Thrust (MCT) at its base and the South Tibetan Detachment (STD) at the top (Fig. 1; Burchfiel et al. 1992; Hodges 2000). The MCT is a first-order tectonic discontinuity in the Himalaya, and an N–S displacement along the thrust is assumed to be more than 140–210 km (e.g., Schelling and Arita 1991; Schelling 1992). The STD is a high-strain, normal fault that traverses nearly the entire length of the Himalaya (e.g., Burchfiel et al. 1992). Many researchers have believed that the contemporaneous and opposing-sense movements along the MCT and the STD caused the exhumation of the HHCS (e.g., Hodges et al. 1992; Grujic et al. 1996; Beaumont et al. 2001; Vannay and Grasemann 2001; Searle et al. 2003; Godin et al. 2006).

The information about the metamorphic evolution of the Himalayan orogen are mainly based on studies of metapelites (Hodges 2000; Vannay and Grasemann 2001 and references therein). The metamorphism in the HHCS had been originally divided in the Eohimalayan stage (the

Editorial Handling: E. Gnos.

T. Imayama (✉)
Department of Earth and Environmental Science, Chonbuk National University, Jeonju 561-756, Republic of Korea
e-mail: t.imayama@gmail.com

intermediate P/T-type metamorphism) of Late Eocene–Oligocene age (38–32 Ma: Vannay and Hodges 1996; Simpson et al. 2000; Godin et al. 2001) and the Neohimalayan stage (high-T at medium- to low-P metamorphism) characterized by widespread anatexis in the Early–Middle Miocene (26–18 Ma: Simpson et al. 2000; Daniel et al. 2003; Viskupic et al. 2005). The later metamorphism is generally associated with movements along the MCT and STD. However, recent reports of Early Oligocene migmatites in the HHCS suggest that Early Oligocene anatexis was widespread in the HHCS than previously thought (Groppo et al. 2010; Imayama et al. 2012; Rubatto et al. 2013; Wang et al. 2013). The Early Oligocene Eohimalayan event is not always characterized by the intermediate-P/T metamorphism (Imayama et al. 2012). Some researchers suggested the upper part of the HHCS uniquely exhumed during Early Oligocene along a shear zone within the HHCS well before the initiation of the activity of the MCT and the STD (Imayama et al. 2012; Carosi et al. 2013; Montomoli et al. 2013). Also, the movement on the MCT occurs as the shear zone with a thickness of a few km (Arita 1983; Harrison et al. 1998). The MCT zone possibly continued until Late Miocene (Kohn et al. 2001; Catlos et al. 2001).

Most studies on the metamorphic evolution of metabasites in the Himalaya focused on the high P/T type eclogites (de Sigoyer et al. 2000; Kaneko et al. 2003; Parrish et al. 2006; Chatterjee and Ghose 2010) and on retrogressed eclogites overprinted by amphibolite–granulite facies metamorphism (Lombardo and Rolfo 2000; Groppo et al. 2007; Liu et al. 2007; Chakungal et al. 2010; Corrie et al. 2010; Kali et al. 2010; Grujic et al. 2011), which were formed during subduction and/or subsequent continent–continent collision. On the other hand, most metabasites exposed in the Himalaya, which occur as the interlayer and tectonic lenses embedded within the metapelites or granites, are normal amphibolite and granulite, not recording eclogite-facies metamorphism. Most of these metabasites are expected to have experienced the same metamorphic history as the regional metapelites, but some authors recently reported that some (not all) metabasite lenses found in metapelites and granite record a unique P–T conditions of an earlier stage and different tectonic event, compared to those recorded in the host rocks (Paudel et al. 2011; Faak et al. 2012; Thakur and Patel 2012). Hence, understanding how non-eclogitic metabasites and host metapelites relate to one another is important key to comprehending the complex tectonics of the shear zone and the polymetamorphic events in the Himalaya.

In this article, the P–T conditions of mafic granulite interlayers and amphibolite blocks within regional metapelites in the far-eastern Nepal Himalaya were studied because the spatial distributions of P–T conditions and metamorphic ages of metapelites in this area have been well documented (Imayama et al. 2010, 2012). The P–T conditions were estimated using pseudosections combined with compositional isopleths of minerals and conventional geothermobarometry. These new P–T data combined with the occurrences of field and microstructures give the tectonic implications for the exhumation process of crustal rocks and kinetic behavior of the shear zone in the Himalaya orogen.

2 Geological setting

The Nepal Himalaya is mainly divided into three tectonic units by north-dipping faults: the Lesser Himalayan Sequence (LHS), the HHCS, and the Tethys Himalayan Sequence (THS) from south to north (Fig. 1). The LHS mainly consists of low- to middle-

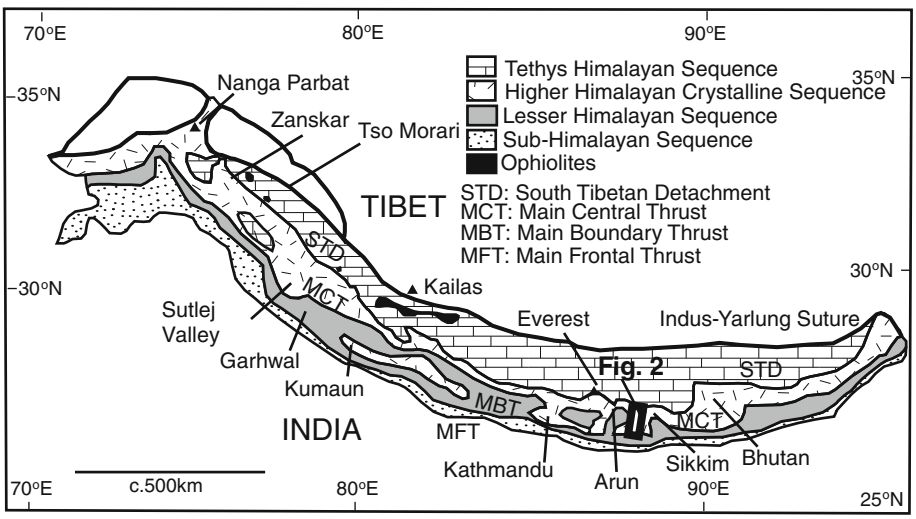

Fig. 1 Simplified geological division of the Himalaya. *Box* in the map shows location of Fig. 2. Modified after Imayama et al. (2012) and references therein

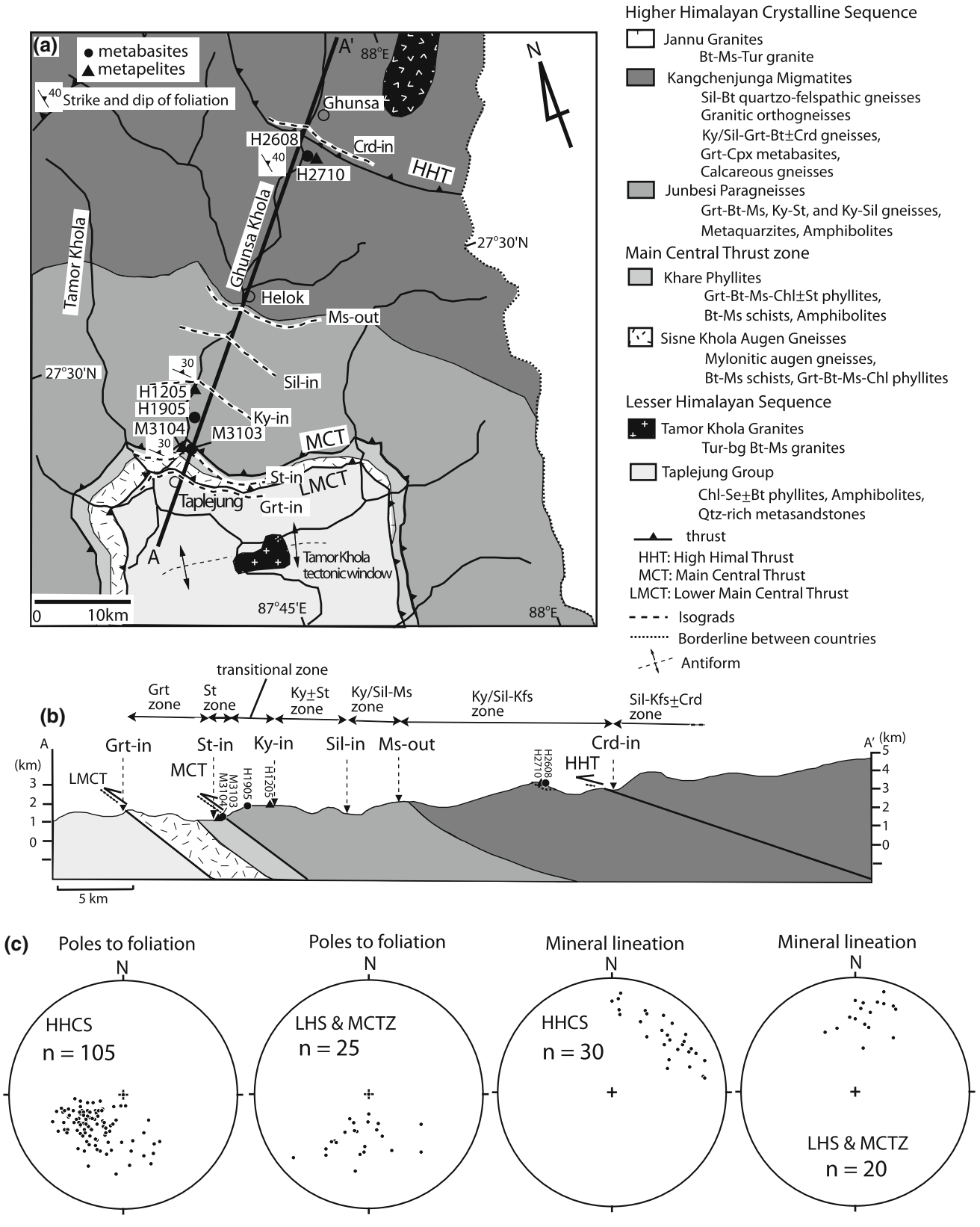

Fig. 2 **a** Geological map and **b** cross section along the Tamor–Ghunsa transect of far-eastern Nepal, showing mineral isograds and locations of mafic samples used for P–T analyses in this study and surrounding metasedimentary samples in Imayama et al. (2010, 2012). **c** Foliation and mineral lineation data from the Tamor–Ghunsa transect. Mineral abbreviations after Kretz (1983)

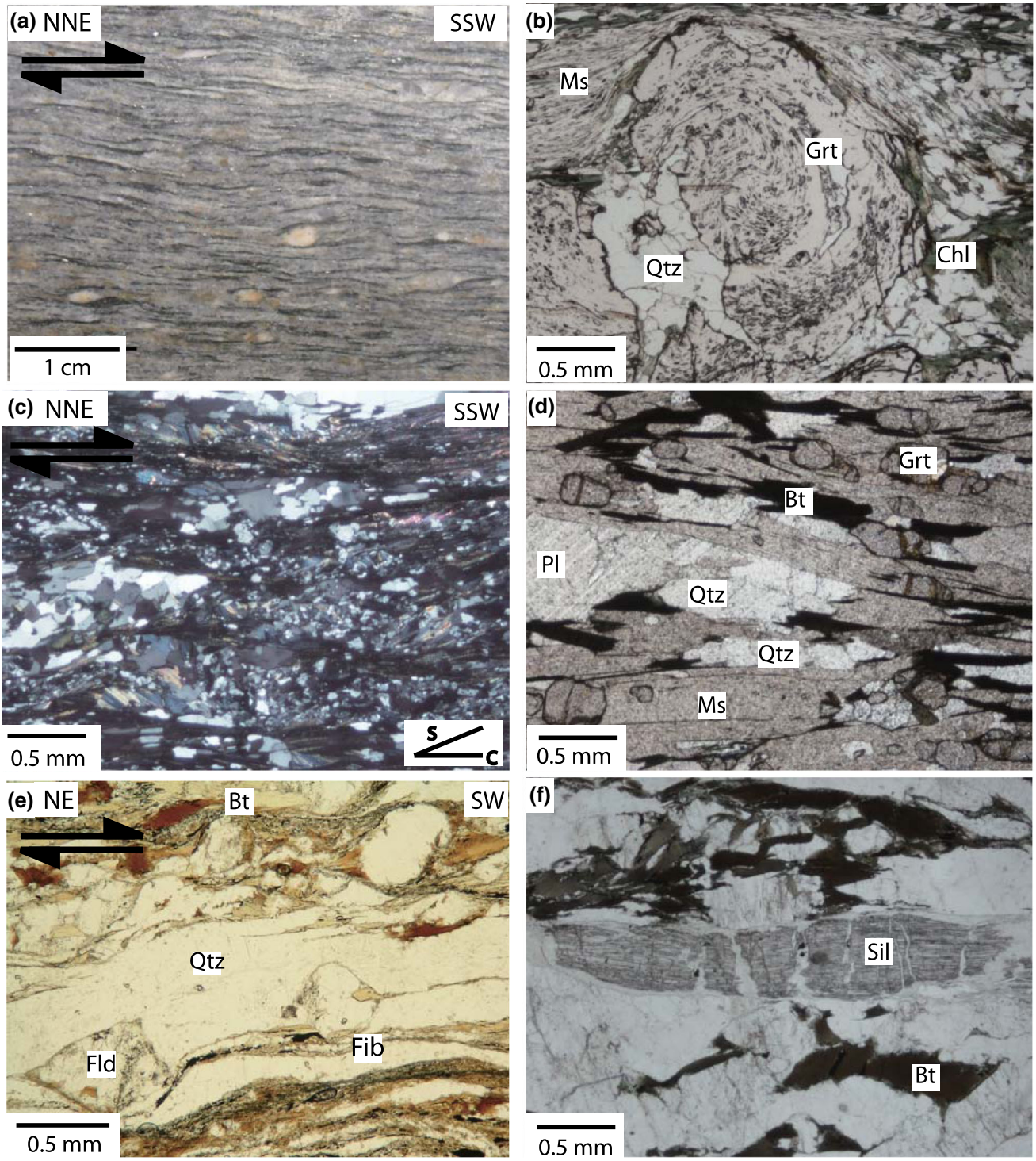

Fig. 3 Photomicrographs of metamorphic rocks near the shear zone in far-eastern Nepal Himalaya. **a** A strong mylonitic foliation of augen gneiss with asymmetric clast-tails of top-to-the-SSW sense in the Sisne Khola Augen Gneisses. **b** S-shaped inclusion train in garnet core in garnet schist of the Khare Phyllites. **c** S–C composite fabrics in garnet schist of the Khare Phyllites, showing a top-to-the-SSW sense of shear. **d** Elongated quartz of garnet–mica gneiss in the Junbesi Paragneisses. **e**. Asymmetric clast-tails and mica fish of sillimanite-bearing mylonitic gneiss near the HHT, showing a top-to-the-SW (thrust) sense of shear. **f** A boudin of sillimanite grain of sillimanite-bearing mylonitic gneiss near the HHT

grade metasediments, and is separated from the overlying high-grade HHCS by the MCT. The HHCS is mainly composed of amphibolite to granulite facies metapelites, leucogranites, and minor metabasites and marbles, and is separated from the overlying THS by the STD. The THS is Early Paleozoic to Early Tertiary sediments (e.g., Brookfield 1993), partly deformed under very low-grade metamorphic conditions (Antolín et al. 2011; Dunkl et al. 2011). The detrital zircon ages from the HHCS show broad age peaks at 2.7–2.3 and 1.3–0.5 Ga, whereas those in the LHS range from 2.6 to 1.6 Ga with a prominent peak at ca. 1.8 Ga (Parrish and Hodges 1996; DeCelles et al. 2000; Richards et al. 2005; Gehrels et al. 2011; McQuarrie et al. 2013). The large differences in $^{143}Nd/^{144}Nd$ values have been also used to characterize provenance (Parrish and Hodges 1996; Robinson et al. 2001; Richards et al. 2005; Imayama and Arita 2008; Tobgay et al. 2010; Motram et al. 2014). The HHCS yields high ε_{Nd} (0) values of −19 to −2, whereas the LHS has ε_{Nd} (0) values of −27 to −16 with exception of the upper LHS rocks showing ε_{Nd} (0) values of −16 to −11 (Ahmad et al. 2000). These U–Pb detrital zircon ages and Nd isotopic data indicate that the protolith ages (Late Proterozoic–Early Paleozoic) of the HHCS are younger than those (Paleoproterozoic–Mesoproterozoic) of the LHS, and the HHCS is not the Indian basement (Parrish and Hodges 1996; DeCelles et al. 2000; Imayama and Arita 2008).

The Tamor–Ghunsa section in far-eastern Nepal crosses the northern part of antiformal Tamor Khola tectonic window of the LHS to the top of the HHCS (Fig. 2). The Tamor Khola Granites occur in the core of a dome and yield U–Pb zircon ages of 1.88–1.85 Ga (Sakai et al. 2013). In the Tamor–Ghunsa section, the most foliation of metamorphic rocks in the HHCS, MCT zone, and LHS strikes NW–SE or NE–SW and dips NE or NW at moderate angles (Fig. 2c). Mineral lineation on the main foliation plunges N–E in the HHCS and NW–NE in the MCT zone and the LHS (Fig. 2c).

Metamorphic peak-T conditions along the section increase upwards from 570 to 670 °C along the MCT, through a significant temperature increase to 740 °C, and reach roughly isothermal conditions (710–810 °C) in the middle part of HHCS (Imayama et al. 2010). Metamorphic pressure conditions at thermal peak increase from 6 to 11 kbar across the MCT, and then decrease up to 7 kbar at the lower part of the HHCS, showing the high metamorphic pressure gradient of 1.2–1.6 kbar/km across the MCT. Subsequently, pressure increases up to secondary peak of ca. 10 kbar near the muscovite-out isograd, and then pressures apparently decrease upwards from 8–10 to 5 kbar in the middle part of the HHCS (Imayama et al. 2010).

2.1 The MCT zone and high himal thrust

In far-eastern Nepal, the MCT is lithologically located between coarse-grained garnet gneiss in the Junbesi Paragneisses of hanging wall and garnet ± staurolite schist in the Khare Phyllites of footwall (Fig. 2a, b). The MCT is

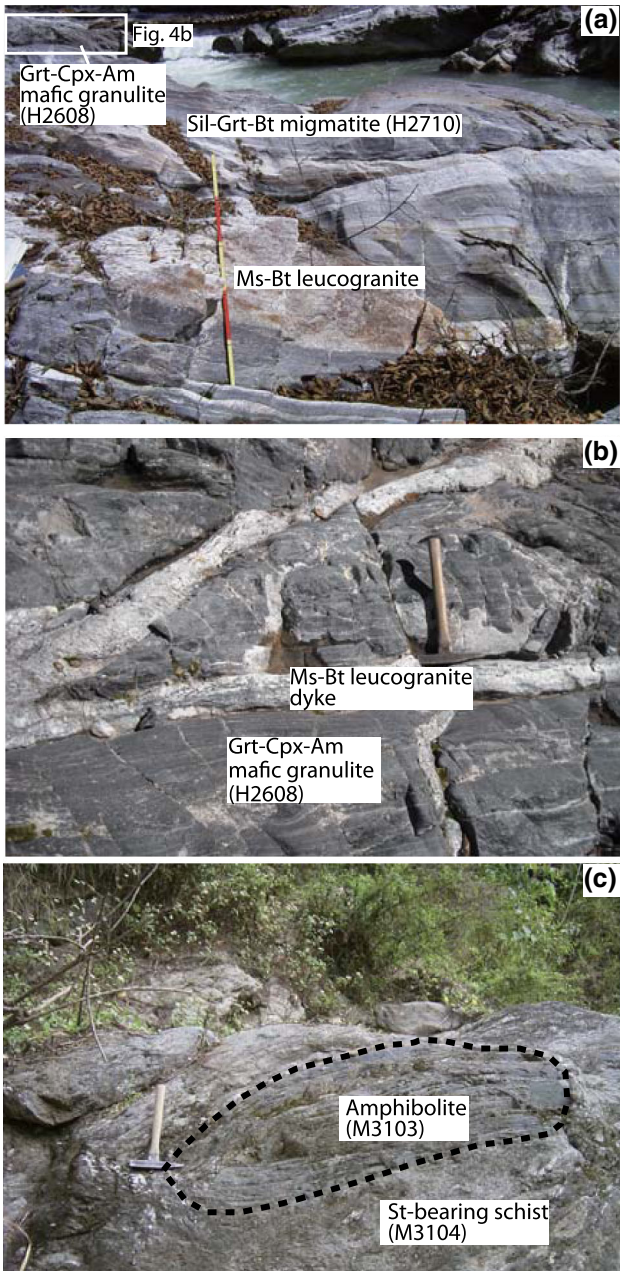

Fig. 4 Outcrop photographs from the Tamor–Ghunsa section, far-eastern Nepal Himalaya. **a** Mafic granulite H2608 intercalated within sillimanite migmatite (sample H2710 of Imayama et al. 2012). **b** Mafic granulite H2608 intruded by muscovite-biotite leucogranite. The foliations in the mafic granulite and sillimanite migmatite are cut by the leucogranites. **c** Amphibolite lense M3103 surrounded by staurolite-bearing schist (sample M3104 of Imayama et al. 2010). *Am* calcic amphibole

Table 1 Representative mineral compositions of amphiboles in metabasites in far-eastern Nepal

Sample	H2608						H1905				M3103			
	Matrix		Matrix		Inclusion in Grt		Matrix		Matrix		Matrix		Matrix	
Spot no.	Core 64	Rim 65	Core 66	Rim 67	41	32	Core 73	Rim 74	Core 87	Rim 88	Core 105	Rim 106	Core 126	Rim 127
SiO_2	43.80	46.09	42.39	45.05	44.15	43.38	44.13	44.14	44.86	43.63	41.24	41.36	41.61	41.69
TiO_2	2.23	1.74	2.40	1.90	1.42	1.42	0.53	0.59	0.49	0.57	0.55	0.52	0.61	0.48
Al_2O_3	11.36	9.89	12.36	10.69	11.59	12.35	12.98	14.32	12.39	13.28	16.14	16.64	15.73	16.58
FeO[a]	15.41	14.55	15.10	14.28	16.59	16.51	16.05	15.88	15.95	16.08	17.43	17.08	17.11	17.01
MnO	0.17	0.17	0.21	0.20	0.25	0.21	0.32	0.28	0.36	0.34	0.27	0.25	0.27	0.29
MgO	10.28	11.21	10.05	11.07	9.72	9.28	9.65	8.76	9.78	9.45	8.28	7.92	8.39	8.02
CaO	11.61	11.88	11.26	11.91	11.38	11.68	11.87	11.33	11.85	11.79	11.22	11.14	11.10	11.46
Na_2O	1.27	1.03	1.49	0.97	1.34	1.13	1.31	1.17	1.42	1.21	1.37	1.41	1.35	1.39
K_2O	0.81	0.40	1.13	0.47	0.69	0.55	0.33	0.75	0.07	0.68	0.30	0.08	0.38	0.05
Total	96.95	96.96	96.38	96.54	97.13	96.50	97.16	97.23	97.15	97.02	96.80	96.39	96.54	96.96
O basis = 46														
Si	6.53	6.80	6.37	6.68	6.56	6.50	6.52	6.52	6.62	6.48	6.10	6.13	6.17	6.16
Al^{IV}	1.47	1.20	1.63	1.32	1.44	1.50	1.48	1.48	1.38	1.52	1.90	1.87	1.83	1.84
Al^{VI}	0.52	0.52	0.55	0.54	0.59	0.67	0.79	1.01	0.78	0.80	0.92	1.04	0.92	1.04
Mg	2.28	2.47	2.25	2.45	2.15	2.07	2.13	1.93	2.15	2.09	1.83	1.75	1.85	1.77
Ti	0.25	0.19	0.27	0.21	0.16	0.16	0.06	0.07	0.05	0.06	0.06	0.06	0.07	0.05
Mn	0.02	0.02	0.03	0.02	0.03	0.03	0.04	0.03	0.04	0.04	0.03	0.03	0.03	0.04
Fe^{3+}	0.22	0.16	0.26	0.20	0.39	0.33	0.37	0.28	0.32	0.36	0.85	0.75	0.78	0.66
Fe^{2+}	1.70	1.63	1.63	1.57	1.68	1.74	1.62	1.68	1.65	1.64	1.31	1.37	1.34	1.44
Ca	1.85	1.88	1.81	1.89	1.81	1.87	1.88	1.79	1.87	1.88	1.78	1.77	1.76	1.81
Na (M4)	0.15	0.12	0.19	0.11	0.19	0.13	0.12	0.21	0.13	0.12	0.22	0.23	0.24	0.19
K	0.15	0.08	0.22	0.09	0.13	0.11	0.06	0.14	0.01	0.13	0.06	0.02	0.07	0.01
Na (A)	0.22	0.17	0.25	0.17	0.20	0.20	0.26	0.13	0.28	0.22	0.17	0.18	0.15	0.21
Sum cations	15.38	15.25	15.46	15.26	15.33	15.31	15.32	15.27	15.30	15.34	15.23	15.19	15.23	15.22
Mg/Mg + Fe	0.57	0.60	0.58	0.61	0.56	0.54	0.57	0.53	0.57	0.56	0.58	0.56	0.58	0.55

[a] Total Fe as FeO

consistent with the gap of Nd isotopic ratio between the LHS and HHCS, indicating the MCT is originally material boundary (Imayama and Arita 2008). Goscombe et al. (2006) argued that the MCT is just an unconformable discontinuity, which may not be a tectonic boundary. However, different P–T paths and high metamorphic pressure gradient across the MCT indicates the MCT is a tectonic boundary related to the activities of the MCT zone (Imayama et al. 2010). In fact, the change of microstructural style along the MCT is observed, as described below.

The lower MCT is placed at the base of the Ulleri-type augen gneiss (Le Fort 1975) in the LHS, which is widely distributed along shear zone of the Nepalese Himalaya (Paudel and Arita 2002; Imayama and Arita 2008). Its thrust corresponds to the MCT of Searle et al. (2008), who defined it as the lower boundary of the MCT zone. In this study, the MCT zone is defined as the sequences between the lower MCT and MCT, and is used as the term of a brittle–ductile shear zone of tectonic boundary between the LHS and HHCS. The MCT zone is divided into two units (Fig. 2a, b). The lowest unit of the MCT zone is the Sisne Khola Augen Gneisses consisting of mylonitic augen gneisses with K-feldspar or albite porphyroclasts. The augen gneiss is characterized by a strong mylonitic foliation, and asymmetric clast-tails show a top-to-the-SSW sense of shear (Fig. 3a). Zircon grains in the augen gneiss have inherited U–Pb ages of ca. 1.86–1.78 Ga (Imayama et al. 2012). The upper unit of the MCT zone, the Khare Phyllites in the LHS, contains garnet ± staurolite phyllites and schists, biotite–muscovite schists, and amphibolites. The phyllites and schists are characterized by S-shaped inclusion train in garnet core (Fig. 3b). A crenulation cleavage in mica is dominant. A shear sense indicator such as S–C composite fabrics in these rocks also indicates a top-to-the-SSW sense of shear (Fig. 3c). The low angle between the S–C planes shows the rock unit is a part of high stain zone.

Table 2 Representative mineral compositions of garnet, clinopyroxene, and plagioclase in metabasites in far-eastern Nepal

Sample	H2608	H2608	H2608	H2608	H2608	H2608	H2608	H1905	H1905	M3103
Mineral	Grt Matrix	Grt	Grt	Cpx Matrix	Cpx Inclusion in Grt	Pl Matrix	Pl	Pl Matrix	Pl	Pl Matrix
	Core	Mantle	Rim			Core	Rim	Core	Rim	
Spot no.	26	19	1	62	4	68	69	91	92	128
SiO_2	38.99	38.52	38.73	52.64	51.60	50.20	48.89	60.74	59.80	59.77
TiO_2	0.07	0.06	0.06	0.01	0.14	0.00	0.00	0.00	0.00	0.00
Al_2O_3	21.60	21.49	21.24	0.48	1.73	31.77	32.54	24.42	25.55	26.18
FeO[a]	24.94	24.65	24.94	11.09	12.36	0.00	0.14	0.01	0.06	0.05
MnO	1.99	1.62	1.55	0.38	0.43	0.00	0.00	0.00	0.00	0.00
MgO	3.81	4.27	4.03	11.94	10.84	0.00	0.00	0.00	0.00	0.00
CaO	9.87	10.01	9.93	23.55	22.61	15.00	15.51	6.16	7.44	7.60
Na_2O	0.01	0.01	0.01	0.14	0.29	3.14	2.70	7.91	7.54	7.04
Total	101.27	100.61	100.47	100.23	100.00	100.10	99.77	99.24	100.40	100.65
O basis	8	8	8	6	6	8	8	8	8	8
Si	3.02	2.99	3.02	1.99	1.96	2.29	2.24	2.72	2.66	2.64
Ti	0.00	0.00	0.00	0.00	0.00	0.00	0.00	0.00	0.00	0.00
Al	1.97	1.97	1.95	0.02	0.08	1.71	1.76	1.29	1.34	1.37
Fe	1.61	1.60	1.63	0.35	0.39	0.00	0.01	0.00	0.00	0.00
Mn	0.13	0.11	0.10	0.01	0.01	0.00	0.00	0.00	0.00	0.00
Mg	0.44	0.49	0.47	0.67	0.61	0.00	0.00	0.00	0.00	0.00
Ca	0.82	0.83	0.83	0.95	0.92	0.73	0.76	0.30	0.35	0.36
Na	0.00	0.00	0.00	0.01	0.02	0.28	0.24	0.69	0.65	0.60
Total	8.00	8.00	8.00	4.01	4.01	5.00	5.00	4.98	5.00	4.98

[a] Total Fe as FeO

The rock unit has been abruptly overlain by coarse-grained garnet gneiss of the Junbesi Paragneisses in the HHCS along the MCT. These gneisses are weakly deformed, and have undergone plastic deformation forming the elongated quartz (Fig. 3d), but they have little mylonitic foliation and asymmetric porphyroblasts as indicator of simple shear. Also, the ptygmatic fold often develops in the Junbesi Paragneisses in contrast to the rocks of the MCT zone.

The High Himal Thrust (HHT), a brittle–ductile shear zone well above the MCT, is found in the middle parts of the HHCS in (far-) eastern Nepal (Fig. 2a, b; Goscombe et al. 2006; Imayama et al. 2010). Goscombe et al. (2006) suggested that the HHT in eastern Nepal is continuous to the MCT in central and western Nepal. However, both thrusts occur at quite different structural level, and the HHT is probably continuous to the shear zone (the High Himalayan discontinuity called by Montomoli et al. 2013) at the higher structural level of the HHCS in western Nepal (Carosi et al. 2010, 2013) and the Nyalam Thrust in southern Tibet (Wang et al. 2013). The HHT mainly consists of sillimanite-bearing mylonitic gneiss. Asymmetric clast-tails and mica fish in the matrix show a top-to-the-SW (thrust) sense of shear (Fig. 3e). The later extensional microstructures such as a boudin of sillimanite grain (Fig. 3f) occur in the rocks near the rocks. These microstructural observations support the idea that the HHT is originally thrust, and then it occurred as extensional fault (Goscombe et al. 2006).

2.2 Sample locations

Mafic granulite H2608 was collected from the middle part of the HHCS above muscovite-out isograd (Fig. 2a, b). It was intercalated within the Early Oligocene sillimanite migmatites (Fig. 4a; sample H2710 of Imayama et al. 2012). The foliations defined by amphibole and plagioclase in the mafic granulite and biotite and sillimanite in the migmatite are parallel strike N30W and dip approximately 40° to the NE. A P–T pseudosection and zircon U–Pb ages of the host migmatites revealed the retrograde path with low P/T gradient from 7–10 kbar, 730–780 °C at 33–28 Ma to 4–7 kbar, 650–725 °C at 27–23 Ma (Imayama et al. 2012). Both mafic granulite and the migmatite are intruded by a muscovite–biotite leucogranite dyke of ca. 18–16 Ma (Fig. 4a, b; Imayama et al. 2012; Imayama and Suzuki 2013).

Sample H1905 was collected from a metabasite block in the sequences above the MCT, which was intercalated with

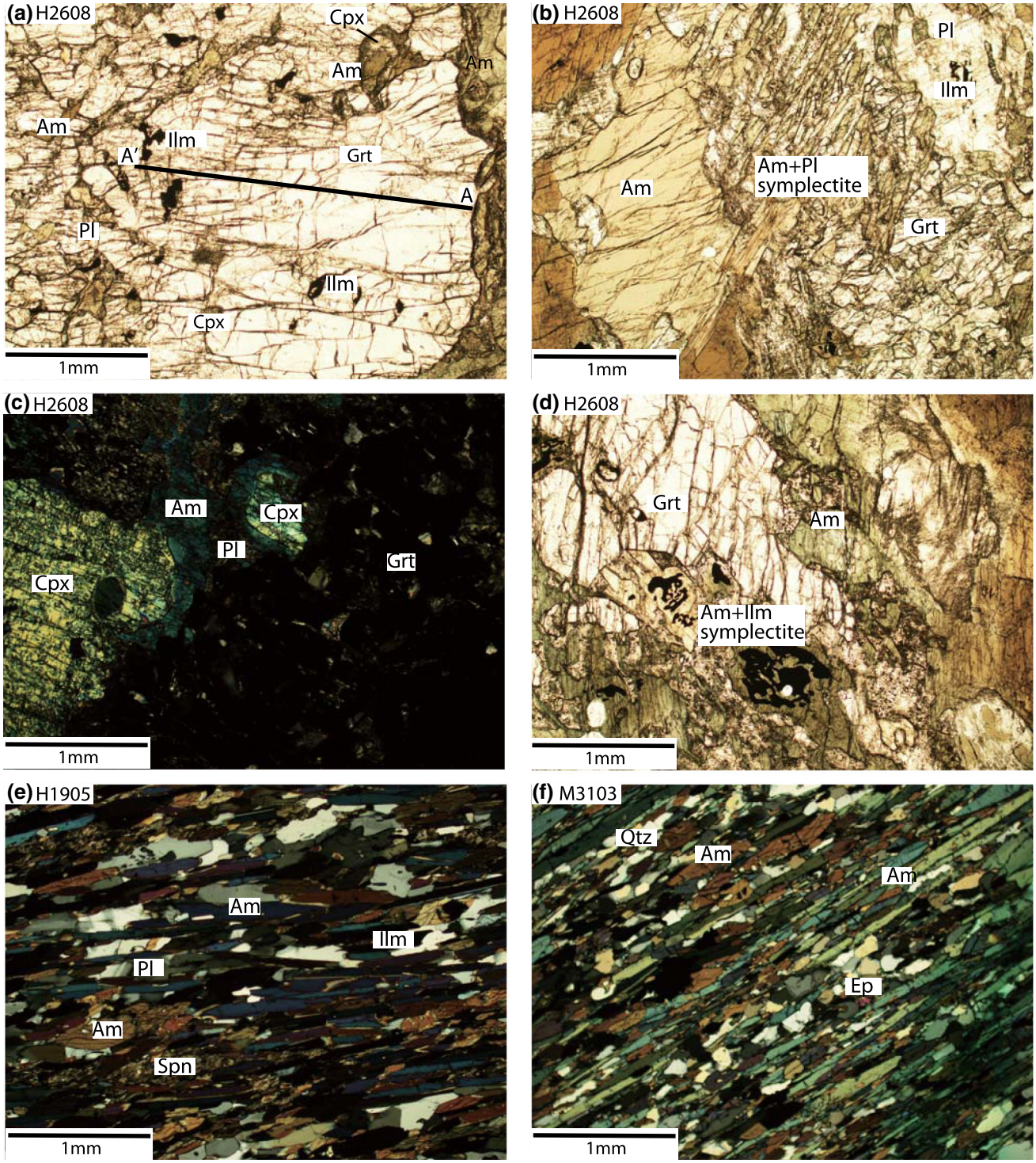

Fig. 5 Photomicrographs of metabasites along the Tamor–Ghunsa section in far-eastern Nepal Himalaya. **a** Garnet porphyroblasts with inclusions of amphibole and ilmenite in the mafic granulite H2608. Compositions along the *black line* are shown in Fig. 7. **b** Symplectites of amphibole + plagioclase surrounding garnet porphyroblast in the mafic granulite H2608. **c** Clinopyroxene partly replaced by symplectic corona of amphibole + plagioclase around its margin in the mafic granulite H2608. **d** Symplectites of amphibole + ilmenite surrounding garnet porphyroblast in the mafic granulite H2608. **e** Highly elongated amphibole and plagioclase defining the foliation in the amphibolite H1905 in the hanging wall of the MCT. **f** Highly elongated amphiboles in the amphibolite M3103 in the footwall of the MCT

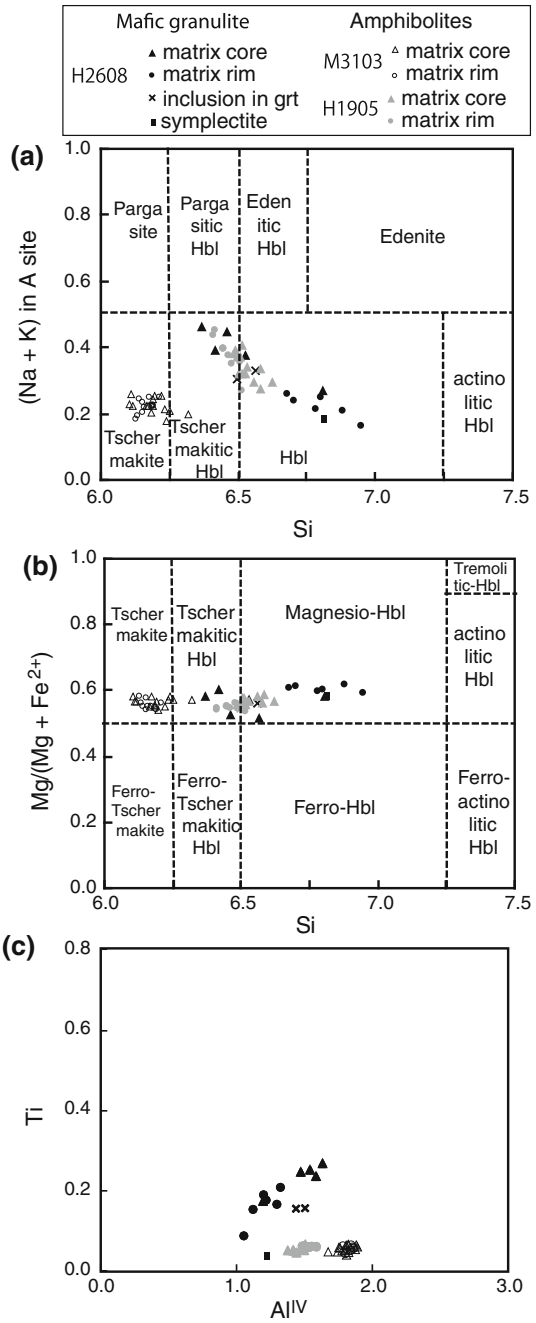

Fig. 6 Classification of Ca-amphiboles according to Leake et al. (1997) for metabasites in far-eastern Nepal, based on **a** (Na + K) in A site-Si diagram and **b** Mg/(Mg + Fe^{2+})-Si diagram. Amphibole compositions plotted in **c** Ti–Al^{IV} diagram

the garnet–mica gneisses (sample H1205 of Imayama et al. 2010, 2012) of the Junbesi Paragneisses at the base of HHCS (Fig. 2a, b). The foliation defined by mica in the garnet-mica gneiss H1205 strikes N70W and dip 30° to the NE, but the direct relationship between the gneiss and amphibolite is unclear. Garnet porphyroblasts in the garnet–mica gneiss preserve their growth zoning, and show a clockwise path with increasing temperature path

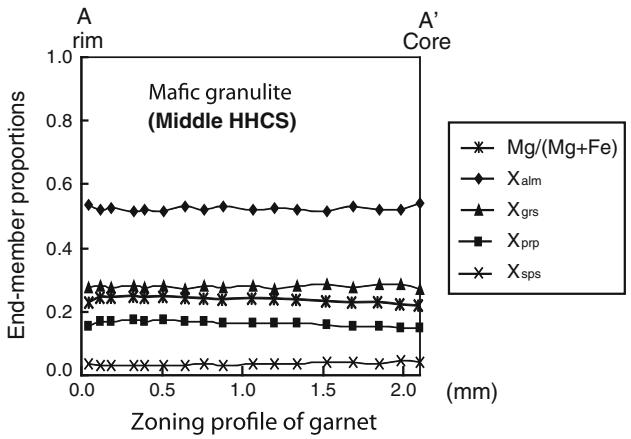

Fig. 7 Compositional zoning profiles of garnet in the mafic granulite H2608 along the Tamor–Ghunsa section in far-eastern Nepal

(590–640 °C) during both loading and decompression following peak pressures of 11–12 kbar (sample H1205 of Imayama et al. 2010). The metamorphic age of garnet–mica gneiss is ca. 25–20 Ma based on U–Pb zircon age (Imayama et al. 2012).

Sample M3103 is an amphibolite lense within staurolite-bearing schists (sample M3104 of Imayama et al. 2010) of the Khare Phyllites in the LHS (Figs. 2a, b, 4c). The amphibolite is strongly elongated parallel to the foliation of the metapelites, implying that they undergo the same deformation events. The foliation strikes N70W and dip 30° to the NE. Mineral lineation of amphibole plunges NNE. In contrast to sample H1205 in hanging wall of the MCT, the staurolite-bearing schist in footwall of the MCT experienced a nearly isothermal loading path, showing the P–T change from 6–7 kbar, 550 °C to 9–10 kbar, 620 °C (Imayama et al. 2010).

3 Petrography and mineral chemistry of metabasites

Mineral compositions were analyzed using a Japanese Electron Optics Laboratory (JEOL) Superprobe 733 electronprobe microanalyser (EPMA) at Hokkaido University. The operating conditions of 15 kV accelerating voltage and 12 nA beam current were used for analyses. Natural and synthetic silicates and oxides were used as standards. Conventional ZAF method was employed for matrix correction. Representative mineral compositions are shown in Tables 1 and 2.

3.1 Mafic granulite H2608

Sample H2608 contains garnet, amphibole, clinopyroxene, biotite, ilmenite, plagioclase, and quartz. Calcite is present

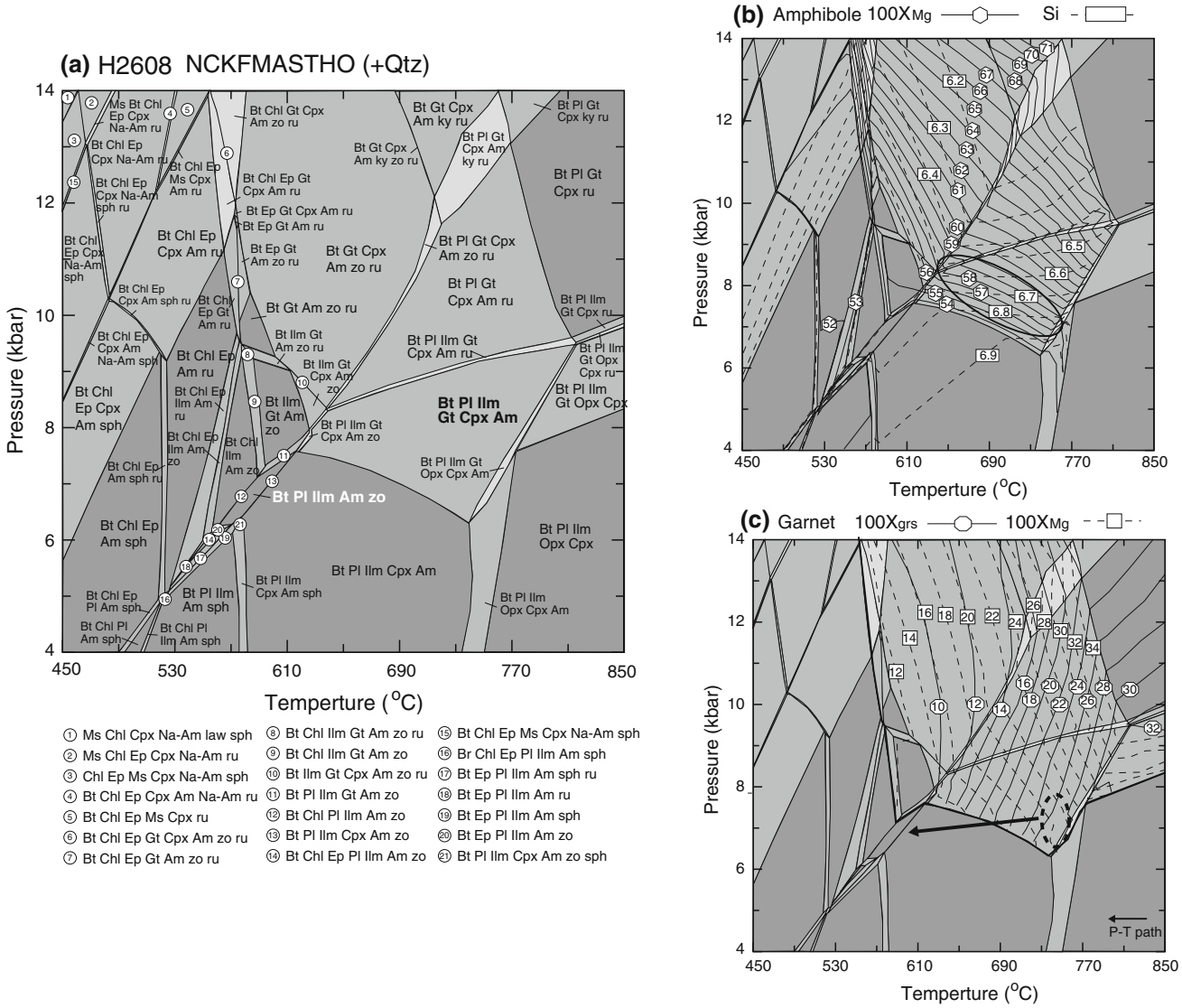

Fig. 8 **a** P–T pseudosections for the mafic granulite H2608 calculated in NCKFMASTHO system. The used bulk compositions (wt%) are SiO_2 (44.81), TiO_2 (1.62), Al_2O_3 (14.39), FeO (12.37), MgO (7.30), CaO (12.00), Na_2O (1.34), K_2O (0.77), and O_2 (0.51). The peak and retrograde assemblages are shown by *black and white bold letters*. **b** Compositional isopleths for amphibole. The amphibole stability is contoured in terms of X_{Mg} and Si content. *Solid ellipse* indicates P–T conditions at which the observed amphibole core composition is reproduced. **c** Compositional isopleths of X_{grs} and X_{Mg} for garnet. *Dashed ellipse* indicates P–T conditions inferred from the observed compositions of garnet. *Na-Am* sodic amphibole

in minor amount. Garnets are large porphyroblasts up to 1 cm in diameter, and include clinopyroxene, amphibole, plagioclase, and ilmenite (Fig. 5a). Symplectite of amphibole + plagioclase occurs at surrounding garnet and clinopyroxene (Fig. 5b, c). Another symplectic amphibole–ilmenite assemblage also occurs at the rim of garnet (Fig. 5d). The crystallization of calcite along fractures and margin in plagioclase reflects the latest metamorphic event at low temperature.

Amphibole in mafic granulite is calcic hornblende with (Na + K) in A site ranging between 0.27 and 0.46 pfu (Fig. 6a; Leake et al. 1997). The Si value (pfu) increases with the decreasing of (Na + K) in A site (Fig. 6a) and the increasing of $Mg/(Mg + Fe^{2+})$ ratio (X_{Mg}; Fig. 6b). Compositional zoning in amphibole is observed, and tschermakitic hornblende core is rimmed by magnesio-hornblend (Fig. 6b). Towards the rim, the X_{Mg} and Si values (pfu) of amphibole increases from 0.53–0.60 to 0.59–0.62 and from 6.4–6.8 to 6.7–7.0 respectively (Fig. 6b). The compositions of amphibole inclusion in garnet and symplectic amphibole surrounding garnet are similar to those of the core and rim of amphibole in matrix, respectively (Fig. 6a, b). From core to rim, Ti and Al^{IV} values decrease (Fig. 6c). Chemical zoning profile in

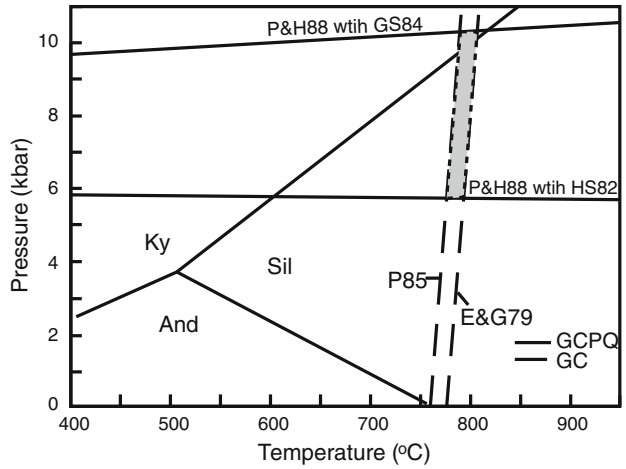

Fig. 9 P–T diagram of the mafic granulite H2608, showing results from the garnet–clinopyroxene (GC) geothermometer (E&G79: Ellis and Green 1979; P85: Powell 1985) and the garnet–clinopyroxene–plagioclase–quartz (GCPQ) geobarometer (P&H88: Powell and Holland 1988). The GCPQ geobarometer from the P&H88 is calculated using the garnet solution models of Hodges and Spear (1982: H&S82) and Ganguly and Saxena (1984: G&S84)

garnet shows a homogenous composition in a crystal, reflecting the zonation modified by diffusion during thermal peak (Fig. 7). Garnet porphyroblasts have high almandine and grossular contents ($X_{Alm} = 0.53–0.54$, $X_{Grs} = 0.26–0.28$) with low pyrope content ($X_{Pyp} = 0.15–0.17$), yielding the X_{Mg} of 0.20–0.22. Calcic clinopyroxene occurs in garnet and matrix. Both clinopyroxene grains are augite with the X_{Mg} of 0.65–0.66 in matrix and 0.60–0.63 in garnet (Table 1). The Na_2O (0.09–0.29 wt%) content of the clinopyroxene is remarkably low. Plagioclase is bytownite, and the composition increases from X_{An} of 0.72–0.73 in core to X_{An} of 0.76–0.78 in rim (Table 1). In contrast, plagioclase in clinopyroxene is $X_{An} = 0.79$.

3.2 Amphibolites H1905 and M3103

Sample H1905 contains amphibole, sphene, plagioclase, quartz, K-feldspar, and ilmenite with minor epidote. Amphibole is strongly elongated (Fig. 5e). Plagioclase is plastically deformed and oriented along the elongation of amphiboles (Fig. 5e). Sphene is common, but epidote is present in minor amount as small grains. Brown amphibole in H1905 is calcic hornblende. The (Na + K) in A site increases with decreasing the Si values (Fig. 6a). The compositions of amphiboles change from magnesio-hornblende in core to tschermakitic-hornblende in rim (Fig. 6b). The X_{Mg} and Si values of amphiboles are 0.56–0.58 and 6.5–6.7 in core and 0.53–0.56 and 6.4–6.5 in rim. The Al^{IV} and Ti values increase slightly from core to rim (Fig. 6c). All analyzed plagioclase grains are zoned, and their composition change from oligoclase ($X_{An} = 0.25–0.30$) to andesine ($X_{An} = 0.35–0.38$) towards the rim.

Sample M3103 contains amphibole, epidote, plagioclase, quartz, and ilmenite. Minor phases are muscovite and chlorite. Chlorite is included in amphibole porphyroblasts. Amphibole is highly elongated (Fig. 5f) and the modal abundance is high (>70 %). Almost all amphibole grains in M3103 are tschermakite (Fig. 6a, b). Amphibole shows low Si values of 6.1–6.5 compared with those of samples H2608 and H1905 (Fig. 6a). The X_{Mg} in amphibole from core to rim is homogenous with compositional range of 0.54–0.58. The Al^{IV} and Ti values do not differ significantly in crystal (Fig. 6c). Plagioclase is andesine ($X_{An} = 0.37$), and is unzoned.

4 P–T analyses

Metamorphic P–T conditions of the mafic granulite H2608 and amphibolites H1905 and M3103 were obtained from pseudosection modeling. The pseudosections were calculated in the chemical system Na_2O–CaO–K_2O–FeO–MgO–Al_2O_3–SiO_2–TiO_2–H_2O–O_2 (NCKFMASTHO) using the Perplex_X program (Connolly 1990) with the internally consistent thermodynamic data set (Holland and Powell 1998; updated in 2002). Quartz and pure H_2O are assumed to be in excess. The Fe^{3+}/Fe^{total} ratio was assumed from the observed mineral assemblages, mode, and mineral compositions: 0.10 for samples H2608 and H1905, and 0.25 for sample M3103. The following solid solution models are used to calculate the pseudosection; garnet (White et al. 2000), biotite (Tajcmanová et al. 2009), muscovite (Chatterjee and Froese 1975), chlorite (Holland et al. 1998), sodic and calcic amphiboles (Dale et al. 2000), clinopyroxene and orthopyroxene (Holland and Powell 1996), epidote (parameters from THERMOCALC), and plagioclase (Newton et al. 1980). Bulk rock compositions used in the pseudosection calculations were analyzed using X-ray fluorescence analysis at Nagoya University.

4.1 Mafic granulite H2608

The pseudosection of the mafic granulite is shown in Fig. 8a. The thermal peak assemblage (garnet + clinopyroxene + amphibole + plagioclase + quartz + ilmenite + biotite + fluid) is stable at the P–T condition of 5–9 kbar, 600–800 °C (Fig. 8a). Although the amount of biotite is minor in the mafic granulite, the pseudosection indicates that biotite is stabilized at a wide P–T area (Fig. 8a). In fact, the absence of muscovite and K-feldspar show that biotite is the stable K_2O phase in the mafic granulite. The amphibole stability is contoured in terms of X_{Mg} and Si value (Fig. 8b). The isopleths of the

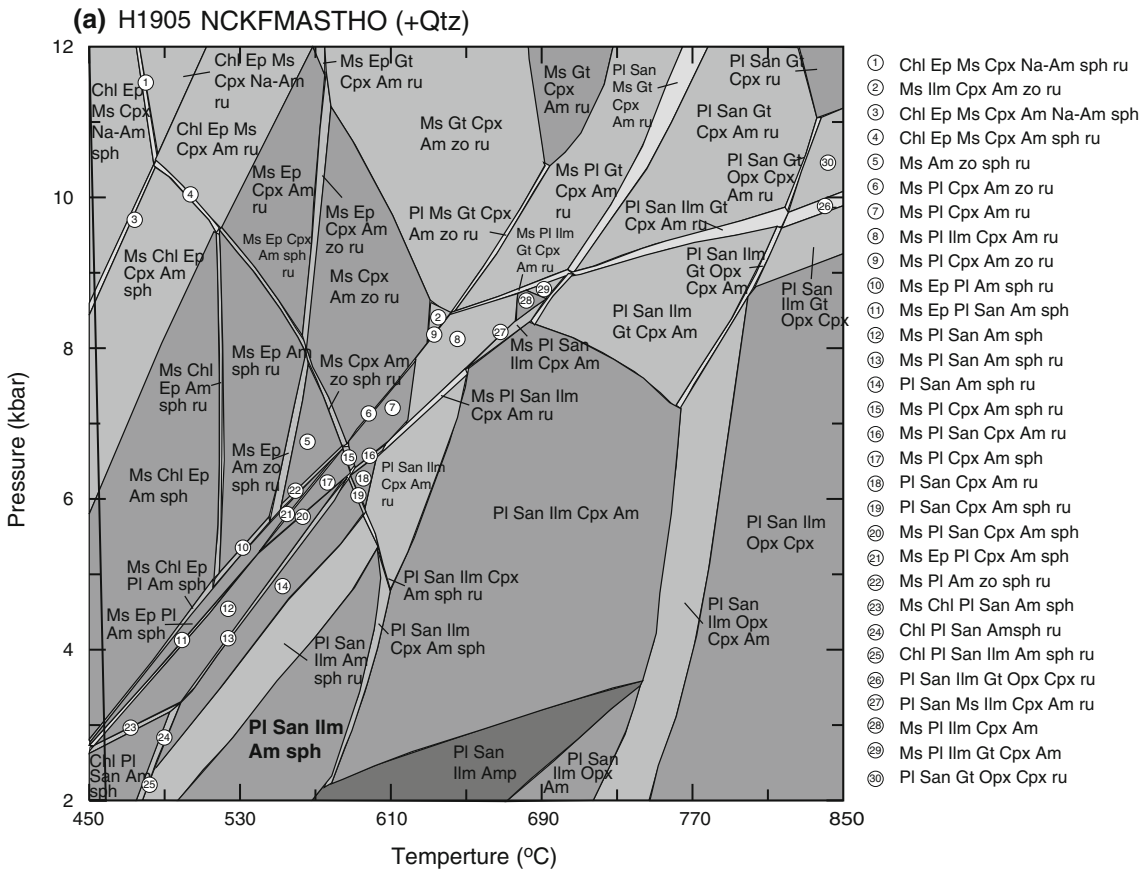
(a) H1905 NCKFMASTHO (+Qtz)
Pressure (kbar)
Temperture (°C)
Chl Ep Ms Cpx Na-Am sph ru
Ms Ilm Cpx Am zo ru
Chl Ep Ms Cpx Am Na-Am sph
Chl Ep Ms Cpx Am sph ru
Ms Am zo sph ru
Ms Pl Cpx Am zo ru
Ms Pl Cpx Am ru
Ms Pl Ilm Cpx Am ru
Ms Pl Cpx Am zo ru
Ms Ep Pl Am sph ru
Ms Ep Pl San Am sph
Ms Pl San Am sph
Ms Pl San Am sph ru
Pl San Am sph ru
Ms Pl Cpx Am sph ru
Ms Pl San Cpx Am ru
Ms Pl Cpx Am sph
Pl San Cpx Am ru
Pl San Cpx Am sph ru
Ms Pl San Cpx Am sph
Ms Ep Pl Cpx Am sph
Ms Pl Am zo sph ru
Ms Chl Pl San Am sph
Chl Pl San Amsph ru
Chl Pl San Ilm Am sph ru
Pl San Ilm Gt Opx Cpx ru
Pl San Ms Ilm Cpx Am ru
Ms Pl Ilm Cpx Am
Ms Pl Ilm Gt Cpx Am
Pl San Gt Opx Cpx ru
Pl San Ilm Am sph
Pl San Ilm Cpx Am sph
Pl San Ilm Amp
Pl San Ilm Opx Am

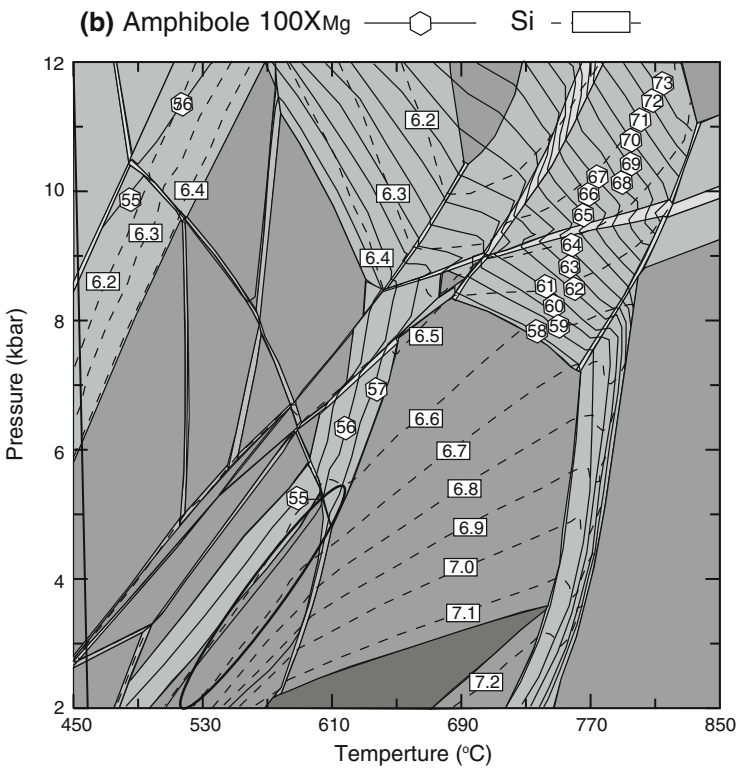
(b) Amphibole 100XMg
Si
Pressure (kbar)
Temperture (°C)

◀**Fig. 10** **a** P–T pseudosections for amphibolite H1905 calculated in NCKFMASTHO system. The used bulk composition (wt%) is SiO_2 (49.23), TiO_2 (1.71), Al_2O_3 (13.60), FeO (10.61), MgO (6.99), CaO (11.23), Na_2O (1.78), K_2O (0.69), and O_2 (0.44). The peak assemblages are shown by *bold letters*. **b** Compositional isopleths of X_{Mg} and Si content for amphibole. *Solid ellipse* indicates P–T conditions inferred from the observed representative compositions of amphibole core

representative core composition ($X_{Mg} = 0.54$–0.60 and Si = 6.5–6.8) in amphibole intersect within the observed phase field, yielding the P–T condition of 6.5–8.5 kbar, 630–750 °C (Fig. 8b). The compositional isopleths of garnet ($X_{Mg} = 0.20$–0.22. $X_{Gls} = 0.26$–0.28) further constrain the thermal peak P–T condition, showing the P–T value of 6.5–8 kbar and 730–750 °C (Fig. 8c).

The retrograde microstructures during later amphibolite facies metamorphism are probably developed according to the following reaction: garnet + clinopyroxene + fluid → amphibole + plagioclase symplectite (or amphibole + plagioclase rims in matrix). The P–T condition at retrograde stage is modeled by the stability field of amphibole + biotite + epidote (zoisite) + plagioclase + quartz + ilmenite + fluid at 6–7.5 kbar, 560–620 °C (Fig. 8a). Hence, the P–T path of mafic granulite is the retrograde path with isobaric cooling (Fig. 8c).

The garnet–clinopyroxene (GC) geothermometer (Ellis and Green 1979; Powell 1985) and garnet–clinopyroxene–plagioclase–quartz (GCPQ) geobarometer (Powell and Holland 1988) are used to compare with the P–T results of the pseudosection. The average composition of garnet core, clinopyroxene inclusion in garnet, and plagioclase inclusion in clinopyroxene are used for the P–T calculation using conventional geothermobarometry. In general, these geothermobarometers have a precision of ±50 °C for temperature and ±1 kbar for pressure. The GCPQ geobarometer and GC geothermometer give the P–T condition of 6–10 kbar, 760–780 °C (Fig. 9), which is roughly similar to those (6.5–8 kbar and 730–750 °C) obtained from the garnet isopleth thermometry within error.

4.2 Amphibolites H1905 and M3103

The P–T pseudosections for two amphibolites are shown in Figs. 10 and 11. Pseudosection of H1905 indicates that the disappearance of sphene occurs at 4–12 kbar, 480–600 °C (Fig. 10a). The peak assemblage of amphibole + plagioclase + sphene + quartz + K-feldspar + ilmenite is predicted in the P–T field at 2–5 kbar, 500–600 °C (Fig. 10a). The representative compositional isopleths of amphibole core ($X_{Mg} = 0.56$–0.57 and Si = 6.6–6.7) intersect within the observed phase field (Fig. 10b). The HP geothermometer (Holland and Blundy 1994) gives the temperatures of 590–620 °C at 4 kbar, which overlaps with the P–T results of the pseudosection.

The bulk composition of sample M3103 has relatively lower MgO and CaO contents, and higher TiO_2 and FeO contents than that of sample H1905. The topology of the pseudosection for M3103 is similar to H1905 in the high temperature region, but the stability fields in the low temperature region are further subdivided (Fig. 11a). The mineral assemblage of amphibole + plagioclase + epidote (zoisite) + chlorite + muscovite + quartz + ilmenite for M3103 is predicted in the P–T field at 6–7.5 kbar, 550–590 °C (Fig. 11a). The isopleths of the representative core composition ($X_{Mg} = 0.54$–0.56 and Si = 6.3–6.5) in amphibole overlapped the P–T phase region (Fig. 11b). The HP geothermometer gives the temperatures of 570–620 °C at 6 kbar, which overlaps with the P–T results of the pseudosection.

5 Discussion

Summary of P–T results from metabasites and surrounding metapelites are given in Table 3. The peak P–T conditions (6.5–8 kbar, 730–750 °C) inferred from garnet isopleth of the mafic granulite H2608 are consistent with those (7–10 kbar, 730–780 °C) of the host sillimanite migmatite (Imayama et al. 2012). This indicates that the mafic granulite was concurrently metamorphosed with the sillimanite migmatite at 33–28 Ma (Imayama et al. 2012). Clearly, the host metapelites are partially melted based on the field observation. In contrast, the degree of partial melting in the mafic granulite is very small. This indicates that the muscovite dehydration reaction easily occurs at the temperatures above 650–700 °C at 5–10 kbar, but amphibole dehydration melting requires higher temperatures of 850–900 °C at 5–10 kbar (Pattison et al. 2003).

After granulite facies metamorphism, these rocks were overprinted by an amphibolite facies metamorphism. The decreasing of the Ti and Al^{IV} values from core to rim in amphiboles in the mafic granulite was interpreted to be retrograde because low Ti and Al^{IV} values in calcic amphibole are generally considered as reliable indicator of low temperatures (Raase 1974; Zenk and Schulz 2004). The occurrence of symplectic amphibole surrounding garnet with similar composition as the amphibole rims (Fig. 5) supports this interpretation. The absence of clinopyroxene + plagioclase symplectite around garnet is in contrast to the Early Miocene granulized eclogites in the Arun area (Lombardo and Rolfo 2000; Groppo et al. 2007). Based on Lu–Hf garnet dating, the eclogite facies metamorphism occurred at 23–16 Ma and was overprinted by thermal peak granulite facies and the later amphibolite facies metamorphisms at ca. 14 Ma in the Arun Valley (Corrie

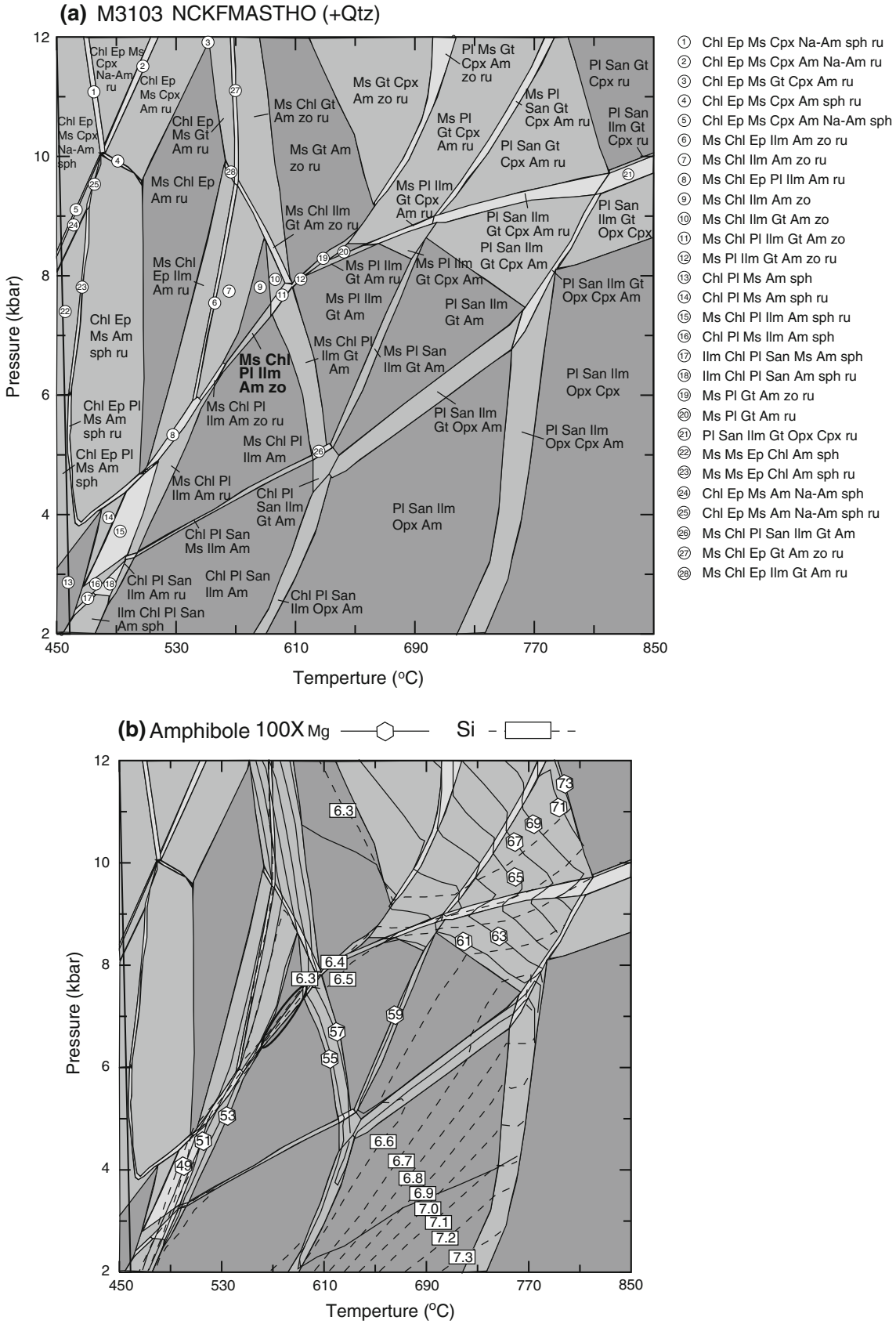
(a) M3103 NCKFMASTHO (+Qtz)
Pressure (kbar)
Temperture (°C)
Chl Ep Ms Cpx Na-Am ru
Chl Ep Ms Cpx Am ru
Chl Ep Ms Cpx Na-Am sph
Chl Ep Ms Gt Am ru
Ms Chl Ep Am ru
Ms Chl Ep Ilm Am ru
Chl Ep Ms Am sph ru
Chl Ep Pl Ms Am sph ru
Chl Ep Pl Ms Am sph
Ms Chl Pl Ilm Am ru
Chl Pl San Ms Ilm Am
Chl Pl San Ilm Am ru
Chl Pl San Ilm Am
Ilm Chl Pl San Am sph
Ms Chl Gt Am zo ru
Ms Gt Cpx Am zo ru
Ms Gt Am zo ru
Ms Chl Ilm Gt Am zo ru
Ms Chl Pl Ilm Am zo ru
Ms Chl Pl Ilm Am
Ms Chl Pl Ilm Gt Am
Chl Pl San Ilm Am
Chl Pl San Ilm Opx Am
Ms Pl Ilm Gt Am ru
Ms Pl Ilm Gt Am
Ms Pl Ilm Gt Cpx Am
Ms Pl Gt Cpx Am ru
Ms Pl San Ilm Gt Am
Pl San Ilm Gt Am
Pl San Ilm Gt Opx Am
Pl Ms Gt Cpx Am zo ru
Ms Pl San Gt Cpx Am ru
Pl San Gt Cpx Am ru
Pl San Ilm Gt Cpx Am ru
Pl San Ilm Gt Cpx Am
Pl San Gt Cpx ru
Pl San Ilm Gt Cpx ru
Pl San Ilm Gt Opx Cpx
Pl San Ilm Gt Opx Cpx Am
Pl San Ilm Opx Cpx
Pl San Ilm Opx Cpx Am
① Chl Ep Ms Cpx Na-Am sph ru
② Chl Ep Ms Cpx Am Na-Am ru
③ Chl Ep Ms Gt Cpx Am ru
④ Chl Ep Ms Cpx Am sph ru
⑤ Chl Ep Ms Cpx Am Na-Am sph
⑥ Ms Chl Ep Ilm Am zo ru
⑦ Ms Chl Ilm Am zo ru
⑧ Ms Chl Ep Pl Ilm Am ru
⑨ Ms Chl Ilm Am zo
⑩ Ms Chl Ilm Gt Am zo
⑪ Ms Chl Pl Ilm Gt Am zo
⑫ Ms Pl Ilm Gt Am zo ru
⑬ Chl Pl Ms Am sph
⑭ Chl Pl Ms Am sph ru
⑮ Ms Chl Pl Ilm Am sph ru
⑯ Chl Pl Ms Ilm Am sph
⑰ Ilm Chl Pl San Ms Am sph
⑱ Ilm Chl Pl San Am sph ru
⑲ Ms Pl Gt Am zo ru
⑳ Ms Pl Gt Am ru
㉑ Pl San Ilm Gt Opx Cpx ru
㉒ Ms Ms Ep Chl Am sph
㉓ Ms Ms Ep Chl Am sph ru
㉔ Chl Ep Ms Am Na-Am sph
㉕ Chl Ep Ms Am Na-Am sph ru
㉖ Ms Chl Pl San Ilm Gt Am
㉗ Ms Chl Ep Gt Am zo ru
㉘ Ms Chl Ep Ilm Gt Am ru
(b) Amphibole 100X Mg Si
Pressure (kbar)
Temperture (°C)
6.3
6.4
6.5
6.6
6.7
6.8
6.9
7.0
7.1
7.2
7.3
73
71
69
67
65
63
61
59
57
55
53
51
49

◀**Fig. 11** **a** P–T pseudosections for amphibolite M3103 calculated in NCKFMASTHO system. The used bulk compositions (wt%) is SiO_2 (48.08), TiO_2 (3.38), Al_2O_3 (13.61), FeO (11.06), MgO (5.48), CaO (9.18), Na_2O (1.31), K_2O (0.33), and O_2 (1.37). The peak assemblages are shown by *bold letters*. **b** Compositional isopleths of X_{Mg} and Si content for amphibole. *Solid ellipse* indicates P–T conditions inferred from the observed representative compositions of amphibole core

et al. 2010). Therefore, the mafic granulite intercalated within the Early Oligocene migmatite has experienced a quite different thermal history than granulized eclogites formed in Early Miocene. Considering that both mafic granulite and Early Oligocene migmatite show a similar retrograde path with low P/T gradient, the mafic granulite was produced by the early subduction and exhumation of the HHCS during Early Oligocene (cf. Imayama et al. 2012). No imprint of the Early Miocene high-grade metamorphism in the mafic granulite supports the idea that the exhumation process of the upper and lower portions of the HHCS occurs as different slices, and the former firstly exhumed along the tectonic discontinuities in the HHCS (Carosi et al. 2010, 2013; Imayama et al. 2012; Montomoli et al. 2013).

The P–T conditions (2–5 kbar, 500–600 °C) of an amphibolite block (sample H1905) above the MCT are significantly lower than that (11–12 kbar, ca. 640 °C) of the surrounding garnet–mica schist (Table 3). The differences in P–T conditions can be interpreted in such a way that the amphibolite (1) records the P–T conditions of an earlier pre-Himalayan metamorphism, (2) was formed during prograde or retrograde stage together with the surrounding garnet–mica gneisses, and (3) is a tectonic block that was metamorphosed at different locations. Pre-Himalayan metamorphism during Early Paleozoic has been reported based on U–Th–Pb ages of monazite grains from metamorphic rocks in central and eastern Nepal (Catlos et al. 2002; Kohn et al. 2004; Gehrels et al. 2006). Although precise P–T conditions during the Early Paleozoic metamorphism are still unknown, the existence of the Early Paleozoic magmatism (Gehrels et al. 2006; Cawood et al. 2007) implies high-temperature condition, incompatible with the low P–T conditions of sample H1905. Whereas the increasing Al^{IV} and Ti values from core to rim in amphibole of sample H1905 are interpreted as prograde zoning (Fig. 5c), the prograde P–T conditions (11 kbar, ca. 590 °C) of the host garnet mica gneiss is quite different (Table 3). Thus, the P–T conditions of sample H1905 cannot represent the prograde or retrograde metamorphism. The amphibolite is strongly deformed like the rocks in the MCT zone (Fig. 5e), whereas the host garnet mica gneiss is relatively little deformed. These occurrences suggest that the amphibolite is part of a tectonic block, accreted from the upper part of MCT zone (i.e. the tectonic mixing of the footwall rocks; Fig. 12) during the movement along the MCT zone. In other words, the amphibolite block was tectonically juxtaposed near the surface with the metapelites of hanging wall when the metapelites of the HHCS exhumed along the MCT zone during the Early–Middle Miocene.

The P–T conditions (6–7.5 kbar, 550–590 °C) obtained on amphibolite lense (sample M3103) below the MCT are similar to prograde P–T conditions, rather than peak P–T conditions (9–10 kbar, ca. 620 °C) of the staurolite–garnet schist in the MCT zone (Table 3). These rocks were metamorphosed together with the activities of the MCT zone during Early–Middle Miocene, as shown by the S-shaped inclusion in garnet in the Khare Phyllites. A high field pressure gradient (1.2–1.6 kbar km) near the MCT (Imayama et al. 2010) is probably caused by ductile deformation of the MCT

Table 3 Summary of P–T results from metabasites and surrounding metapelites

Sample #	Rock type	Location	Prograde	Peak	Retrograde	References
M3104	Staurolite–garnet schist	Near MCT	6–7 kbar, ca. 550 °C^{G}	9-10 kbar, ca. 620 °C$^{P,\ G,A,C}$		Imayama et al. (2010)
M3103	Amphibolite	Near MCT	6–7.5 kbar, 550–590 °C^{P,C}			This study
H1905	Amphibolite	Base of the HHCS		2–5 kbar, 500–600 °C^{P,C}		This study
H1205	Garnet–mica gneiss	Base of the HHCS	11 kbar, ca. 590 °C^{G}	11–12 kbar, ca. 640 °C^{G,A,C} at 25–20 Ma		Imayama et al. (2010, 2012)
H2710	Sillimanite migmatite	Near HHT		7–10 kbar, 730–780 °C^{P} at 33–28 Ma	4–7 kbar, 650–725 °C^{P} at 27–23 Ma	Imayama et al. (2012)
H2608	Mafic granulite	Near HHT		6.5–8 kbar, 730–750 °C^{P,C}	6–7.5 kbar, 560–620 °C^{P}	This study

P–T conditions are estimated using pseudosection modeling (P), average-P–T method (A), Gibbs method (G), and conventional geothermometer (C)

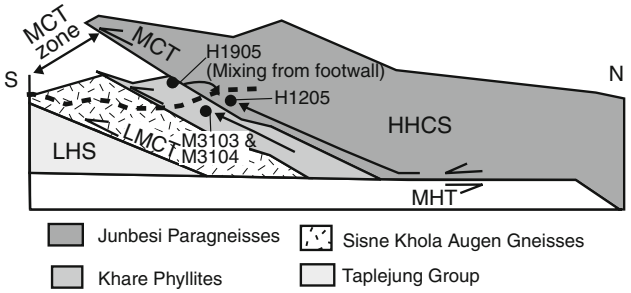

Fig. 12 A schematic cartoon of the tectonic model on the MCT zone. *Dashed line* shows a surface topography

zone, not the emplacement along a single thrust (Fig. 12). This study indicates the top-to-the south movement of the MCT zone results in the tectonic assembly of rocks with different P–T–t paths near the MCT (cf. Jamieson et al. 2004; Imayama et al. 2010), but additional high-precision age data from metabasites within the metapelites are needed in order to understand the precise timing and nature of the MCT zone.

6 Conclusions

Metamorphic evolution of the metabasites in far-eastern Nepal has been investigated using pseudosection modeling and conventional geothermobarometry. The mafic granulite that is intercalated within the Early Oligocene migmatite at the center of the HHCS was metamorphosed at similar P–T conditions (6.5–8 kbar, 730–750 °C) as the host rocks, indicating they were simultaneously metamorphosed during the Early Oligocene. In contrast, metabasite block above the MCT yielded P–T condition of 2–5 kbar, 500–600 °C, different from the 7–10 kbar, 730–780 °C of the surrounding Early Miocene metasediments. Considering that the amphibolite is strongly deformed like rocks in the footwall of MCT, it might be a tectonic block that accreted from the upper part of MCT zone during the movement of the MCT zone. The P–T conditions of amphibolite below the MCT are 6–7.5 kbar, 550–590 °C, which is similar to prograde P–T conditions of surrounding staurolite–garnet schist. Both rocks were metamorphosed together during the Early–Middle Miocene activities of the MCT zone.

Acknowledgments The author greatly appreciates Dr. K. Suzuki (Nagoya University) for kind assistance with XRF analyses. I wish to thank Dr. K. S. Yengkhom (Chonbuk National University) for useful discussion on this study. I appreciate the reviews by Dr. C. Montomoli and Dr. A. El Korh, which have greatly improved the quality of manuscript. The author also thanks Dr. E. Gnos, for editorial handling of the manuscript and correction of the English text.

References

Ahmad, T., Harris, N., Bickle, M., Chapman, H., Bunbury, J., & Prince, C. (2000). Isotopic constraints on the structural relationships between the Lesser Himalayan Series and the High Himalayan Crystalline Series, Garhwal Himalaya. *Geological Society of America Bulletin, 112*, 467–477.

Antolín, B., Appel, A., Montomoli, C., Dunkl, I., Ding, L., Gloaguen, R., & El Bay, R. (2011). Kinematic evolution of the eastern Tethyan Himalaya: constraints from magnetic fabric and structural properties of the Triassic flysch in SE Tibet. In J. Poblet & R. Lisle (Eds.), *Kinematic Evolution and Structural Styles of Fold-and-Thrust Belts*, vol 349 (pp. 99–121). London: Geological Society of London Special Publications.

Arita, K. (1983). Origin of the inverted metamorphism of the Lower Himalayas, central Nepal. *Tectonophysics, 95*, 43–60.

Beaumont, C., Jamieson, R. A., Nguyen, M. H., & Lee, B. (2001). Himalayan tectonics explained by extrusion of a low-viscosity crustal channel coupled to focused surface denudation. *Nature, 414*, 738–742.

Brookfield, M. E. (1993). The Himalayan passive margin from Precambrian to Cretaceous. *Sedimentary Geology, 84*, 1–35.

Burchfiel, B. C., Chen, Z., Hodges, K. V., Liu, Y., Royden, L. H., Deng, C., et al. (1992). The south Tibetan detachment system, Himalayan orogen: extension contemporaneous with and parallel to shortening in a collisional mountain belt. *Geological Society of America Special Paper, 269*, 1–41.

Carosi, R., Montomoli, C., Rubatto, D., & Visona, D. (2013). Leucogranite intruding the South Tibetan Detachment in western Nepal: implications for exhumation models in the Himalayas. *Terra Nova,*. doi:10.1111/ter.12062.

Carosi, R., Montomoli, C., Rubatto, D., & Visonà, D. (2010). Late Oligocene high-temperature shear zones in the core of the Higher Himalayan Crystallines (Lower Dolpo, Western Nepal). *Tectonics, 29*, 4029. doi:10.1029/2008TC002400.

Catlos, E. J., Harrison, T. M., Kohn, M. J., Grove, M., Ryerson, F. J., Manning, C. E., et al. (2001). Geochronologic and thermobarometric constraints on the evolution of the Main Central Thrust, central Nepal Himalaya. *Journal of Geophysical Research, 106*, 16177–16204.

Catlos, E. J., Harrison, T. M., Manning, C. E., Grove, M., Rai, S. M., Hubbard, M. S., et al. (2002). Records of the evolution of the Himalayan orogen from in situ Th–Pb ion microprobe dating of monazite: Eastern Nepal and western Garhwal. *Journal of Asian Earth Science, 20*, 459–479.

Cawood, P. A., Johnson, M. R. W., & Nemchin, A. A. (2007). Early Paleozoic orogenesis along the Indian margin of Gondwana: tectonic response to Gondwana assembly. *Earth and Planetary Science Letters, 255*, 70–84.

Chakungal, J., Dostal, J., Grujic, D., Duchêne, S., & Ghalley, S. K. (2010). Provenance of the Greater Himalayan Sequence: evidence from mafic eclogite-granulites and amphibolites in NW Bhutan. *Tectonophysics, 480*, 198–212.

Chatterjee, N. D., & Froese, E. (1975). A thermodynamic study of the pseudo-binary join muscovite–paragonite in the system $KAlSi_3O_8$–$NaAlSi_3O_8$–Al_2O_3–SiO_2–H_2O. *American Mineralogist, 60*, 985–993.

Chatterjee, N., & Ghose, N. C. (2010). Metamorphic evolution of the Naga Hills eclogite and blueschist, Northeast India: implications for early subduction of the Indian plate under the Burma microplate. *Journal of Metamorphic Geology, 28*, 209–225.

Connolly, J. A. D. (1990). Multivariable phase diagrams: an algorithm based on generalized thermodynamics. *American Journal of Science, 290*, 666–718.

Corrie, S. L., Kohn, M. J., & Vervoort, J. D. (2010). Young eclogite from the Greater Himalayan Sequence, Arun Valley, eastern Nepal: P–T–t path and tectonic implications. *Earth Planetary Science Letters, 289*, 406–416.

Dale, J., Holland, T., & Powell, R. (2000). Hornblende-garnet-plagioclase thermobarometry: a natural assemblage calibration of the thermodynamics of hornblende. *Contributions to Mineralogy and Petrology, 140*, 353–362.

Daniel, C. G., Hollister, L. S., Parrish, R. R., & Grujic, D. (2003). Exhumation of the Main Central Thrust from lower crustal depths, eastern Bhutan Himalaya. *Journal of Metamorphic Geology, 21*, 317–334.

de Sigoyer, J., Chavagnac, V., Blichert-Toft, J. J., Villa, I. M., Luais, B., Guillot, S., et al. (2000). Dating continental subduction and collisional thickening in NW Himalaya: multichronometry of the Tso Morari eclogites. *Geology, 28*, 487–490.

DeCelles, P. G., Gehrels, G. E., Quade, J., LeReau, B., & Spurlin, M. (2000). Tectonic implications of U–Pb zircon ages of the Himalayan orogenic belt in Nepal. *Science, 288*, 497–499.

Dunkl, I., Antolín, B., Wemmer, K., Rantitsch, G., Kienast, M., Montomoli, C., Ding, L., Carosi, R., Appel, E., El Bay, R., Xu, Q., & Von Eynatten, H. (2011). Metamorphic evolution of the Tethyan Himalayan flysch in SE Tibet. In Gloaguen, R., & Ratschbacher, L. (Eds.) *Growth and Collapse of the Tibetan Plateau*, vol 353 (pp. 45–69). London: Geological Society, London, Special Publications.

Ellis, D. J., & Green, E. H. (1979). An experimental study of the effect of Ca upon garnet–clinopyroxene Fe–Mg exchange equilibria. *Contributions to Mineralogy and Petrology, 71*, 13–22.

Faak, K., Chakraborty, S., & Dasgupta, S. (2012). Petrology and tectonics significance of metabasites slivers in the lesser and higher Himalayan domains of Sikkim, India. *Journal of Metamorphic Geology, 30*, 599–622.

Ganguly, J., & Saxena, S. K. (1984). Mixing properties of aluminosilicate garnets: constraints from natural and experimental data, and applications to geothermobarometry. *American Mineralogist, 69*, 88–97.

Gehrels, G. E., DeCelles, P. G., Ojha, Y. P., & Upreti, B. N. (2006). Geologic and U–Th–Pb geochronologic evidence for early Paleozoic tectonism in the Kathmandu thrust sheet, central Nepal Himalaya. *Geological Society of America Bulletin, 118*, 185–198.

Gehrels, G., Kapp, P., DeCelles, P., Pullen, A., Blakey, R., Weislogel, A., et al. (2011). Detrital zircon geochronology of pre-Tertiary strata in the Tibetan–Himalayan orogen. *Tectonics,*. doi:10.1029/2011TC002868.

Godin, L., Grujic, D., Law, R. D., & Searle, M. P. (2006). Channel flow, ductile extrusion and exhumation in continental collision zones: an introduction. In R. D. Law, M. P. Searle, & L. Godin (Eds.), *Channel Flow, Ductile Extrusion and Exhumation in Continental Collision Zones, Special Publications 268* (pp. 1–23). London: Geological Society.

Godin, L., Parrish, R. R., Brown, R. L., & Hodges, K. V. (2001). Crustal thickening leading to exhumation of the Himalayan metamorphic core of central Nepal: insight from U–Pb geochronology and $^{40}Ar/^{39}Ar$ thermochronology. *Tectonics, 20*, 729–747.

Goscombe, B., Gray, D., & Hand, M. (2006). Crustal architecture of the Himalayan metamorphic front in eastern Nepal. *Gondwana Research, 10*, 232–255.

Groppo, C., Lombardo, B., Rolfo, F., & Pertusati, P. (2007). Clockwise exhumation path of granulized eclogites from the Ama Drima range (Eastern Himalayas). *Journal of Metamorphic Geology, 25*, 51–75.

Groppo, C., Rubatto, D., Rolfo, F., & Lombardo, B. (2010). Early Oligocene partial melting in the Main Central Thrust zone (Arun valley, eastern Nepal Himalaya). *Lithos, 118*, 287–301.

Grujic, D., Casey, M., Davidson, C., Hollister, L. S., Kundig, R., Parvlis, T., et al. (1996). Ductile extrusion of the higher Himalayan crystalline in Bhutan: evidence from quartz microfabrics. *Tectonophysics, 260*, 21–43.

Grujic, D., Warren, C. J., & Wooden, J. L. (2011). Rapid synconvergent exhumation of Miocene-aged lower orogenic crust in the eastern Himalaya. *Lithosphere, 3*, 346–366.

Harrison, T. M., Grove, M., Lovera, O. M., & Catlos, E. J. (1998). A model for the origin of Himalayan anatexis and inverted metamorphism. *Journal of Geophysical Research, 103*(B11), 27017–27032.

Hodges, K. V. (2000). Overview: tectonics of the Himalaya and southern Tibet from two perspectives. *Geological Society of America Bulletin, 112*, 324–350.

Hodges, K. V., Parrish, R. R., Housh, T. B., Lux, D. R., Burchfiel, B. C., Royden, L. H., et al. (1992). Simultaneous Miocene extension and shortening in the Himalayan Orogen. *Science, 258*, 1466–1470.

Hodges, K. V., & Spear, F. S. (1982). Geothermometry, geobarometry and the Al_2SiO_5 triple point at Mt. Moosilauke, New Hampshire. *American Mineralogist, 67*, 1118–1134.

Holland, T., Baker, J., & Powell, R. (1998). Mixing properties and activity-composition relationships of chlorites in the system $MgO–FeO–Al_2O_3–SiO_2–H_2O$. *European Journal of Mineralogy, 10*, 395–406.

Holland, T. J. B., & Blundy, J. (1994). Non-ideal interactions in calcic amphiboles and their bearing on amphibole-plagioclase thermometry. *Contributions to Mineralogy and Petrology, 116*, 433–447.

Holland, T., & Powell, R. (1996). Thermodynamics of order–disorder in minerals. 2. Symmetric formalism applied to solid solutions. *American Mineralogist, 81*, 1425–1437.

Holland, T. J. B., & Powell, R. (1998). An internally consistent thermodynamic data set for phases of petrological interest. *Journal of Metamorphic Geology, 16*, 309–343.

Imayama, T., & Arita, K. (2008). Nd isotopic data reveal the material and tectonic nature of the Main Central Thrust zone in Nepal Himalaya. *Tectonophysics, 451*, 265–281.

Imayama, T., & Suzuki, K. (2013). Carboniferous inherited grain and age zoning of monazite and xenotime from leucogranites in far-eastern Nepal: constraints from electron probe microanalysis. *American Mineralogist, 98*, 1393–1406.

Imayama, T., Takeshita, T., & Arita, K. (2010). Metamorphic P–T profile and P–T path discontinuity across the far-eastern Nepal Himalaya: investigation of channel flow models. *Journal of Metamorphic Geology, 28*, 527–549.

Imayama, T., Takeshita, T., Yi, K., Cho, D. L., Lee, Y., Kitajima, K., et al. (2012). Two-stage partial melting and contrasting cooling rates within the higher Himalayan crystalline sequences in the far-eastern Nepal Himalaya. *Lithos, 134–135*, 1–22.

Jamieson, R. A., Beaumont, C., Medvedev, S., & Lee, B. (2004). Crustal channel flows: 2. Numerical models with implications for metamorphism in the Himalayan–Tibetan orogen. *Journal of Geophysical Research, 109*, B06407. doi:10.1029/2003JB002811.

Kali, E., Leloup, P. H., Arnaud, N., Mahéo, G., Liu, D., Boutonnet, E., et al. (2010). Exhumation history of the deepest central Himalayan rocks, Ama Drime range: key pressure–temperature–deformation–time constraints on orogenic models. *Tectonics, 29*, TC2014. doi:10.1029/2009TC002551.

Kaneko, Y., Katayama, I., Yamamoto, H., Misawa, K., Ishikawa, M., Rewman, H. U., et al. (2003). Timing of Himalayan ultrahigh-pressure metamorphism: sinking rate and subduction angle of the Indian continental crust beneath Asia. *Journal of Metamorphic Geology, 21*, 589–599.

Kohn, M. J., Catlos, E. J., Ryerson, F. J., & Harrison, T. M. (2001). Pressure–temperature–time path discontinuity in the Main Central Thrust zone, central Nepal. *Geology, 29*, 571–574.

Kohn, M. J., Wieland, M. S., Parkinson, C. D., & Upreti, B. N. (2004). Miocene faulting at plate tectonic velocity in the Himalaya of central Nepal. *Earth Planetary Science Letters, 228*, 299–310.

Kretz, R. (1983). Symbols for rock-forming minerals. *American Mineralogist, 68*, 277–279.

Le Fort, P. (1975). Himalayas: the collided range. Present knowledge of the continental arc. *American Journal Science, 275A*, 1–44.

Leake, B. E., Woolley, A., Arps, C. E. S., Birch, W. D., Gilbert, M. C., Grice, J. D., et al. (1997). Nomenclature of amphiboles: report of the subcommittee on amphiboles of the International Mineralogical Association, commission on new minerals and mineral names. *American Mineralogist, 82*, 1019–1037.

Liu, Y., Siebel, W., Massonne, H. J., & Xiao, X. C. (2007). Geochronological and petrological constraints for tectonic evolution of the central Greater Himalayan sequence in the Kharta area, southern Tibet. *The Journal of Geology, 115*, 215–230. doi:10.1086/510806.

Lombardo, B., & Rolfo, F. (2000). Two contrasting eclogite types in the Himalayas: implications for the Himalayan orogeny. *Journal of Geodynamics, 30*, 37–60.

McQuarrie, N., Long, S. P., Tobgay, T., Nesbit, J. N., Gehrels, G., & Ducea, M. N. (2013). Documenting basin scale, geometry and provenance through detrital geochemical data: lessons from the Neoproterozoic to Ordovician Lesser, Greater, and Tethyan Himalayan strata of Bhutan. *Gondwana Research, 23*, 1491–1510.

Montomoli, C., Iaccarino, S., Carosi, R., Langone, A., & Visona, D. (2013). Tectonometamorphic discontinuities within the Greater Himalayan sequence in Western Nepal (Central Himalaya): insights on the exhumation of crystalline rocks. *Tectonophysics, 608*, 1349–1370. doi:10.1016/j.tecto.2013.06.006.

Motram, C. M., Argles, T. W., Harris, N. B. W., Parish, P. R., Horstwod, M. S. A., Waren, C. J., et al. (2014). Tectonic interleaving along the Main Central Thrust, Sikkim Himalaya. *Journal of the Geological Society London, 171*, 255–268.

Newton, R. C., Charlu, T. V., & Kleppa, O. J. (1980). Thermochemistry of the high structural state plagioclases. *Geochimica Cosmochimica Acta, 44*, 933–941.

Parrish, R. R., Gough, S. J., Searle, M. P., & Waters, D. J. (2006). Plate velocity exhumation of ultrahigh-pressure eclogites in the Pakistan Himalaya. *Geology, 34*, 989–992.

Parrish, R. R., & Hodges, K. V. (1996). Isotopic constrains on the age and provenance of the Lesser and Greater Himalayan sequences, Nepalese Himalaya. *Geological Society of America Bulletin, 108*, 904–911.

Pattison, D. R. M., Chacko, T., Farquhar, J. F., & McFarlane, C. R. M. (2003). Temperatures of granulite-facies metamorphism: constrains from experimental phase equilibria and thermobarometry corrected for retrograde exchange. *Journal of Petrology, 44*, 867–900.

Paudel, L. P., & Arita, K. (2002). Locating the Main Central Thrust in central Nepal using lithologic, microstructural and metamorphic criteria. *Journal of Nepal Geological Society, 26*, 29–42.

Paudel, L. P., Imayama, T., & Arita, K. (2011). Metabasites petrology and P–T evolution in the Lesser Himalaya, central Nepal. *Journal of Nepal Geological Society, 42*, 21–38.

Powell, R. (1985). Regression diagnostics and robust regression in geothermometer/geobarometer calibration: the garnet–clinopyroxene geothermometer revisited. *Journal of Metamorphic Geology, 3*, 231–243.

Powell, R., & Holland, T. J. B. (1988). An internally consistent thermodynamic dataset with uncertainties and correlations: 3. Applications to geobarometry, worked examples and a computer program. *Journal of Metamorphic Geology, 6*, 173–204.

Raase, P. (1974). Al and Ti contents of hornblende, indicators of pressure and temperature of regional metamorphism. *Contributions to Mineralogy and Petrology, 45*, 231–236.

Richards, A., Argles, T., Harris, N., Parrish, R., Ahmad, T., Darbyshire, F., et al. (2005). Himalayan architecture constrained by isotopic tracers from clastic sediments. *Earth Planetary Science Letters, 236*, 773–796.

Robinson, D. M., DeCelles, P. G., Patchett, P. J., & Garzion, C. N. (2001). The kinematic evolution of the Nepalese Himalaya interpreted from Nd isotopes. *Earth Planetary Science Letters, 192*, 507–521.

Rubatto, D., Chakraborty, S., & Dasgupta, S. (2013). Timescales of crustal melting in the Higher Himalayan crystallines (Sikkim, Eastern Himalaya) inferred from trace element-constrained monazite and zircon chronology. *Contributions to Mineralogy and Petrology, 165*, 349–372.

Sakai, H., Iwano, H., Danhara, T., Takigami, Y., Rai, S. M., Upreti, B. N., et al. (2013). Rift-related origin of the Paleoproterozoic Kuncha Formation, and cooling history of the Kuncha nappe and Taplejung granites, eastern Nepal Lesser Himalaya: a multi-chronological approach. *Island Arc, 22*, 338–360.

Schelling, D. (1992). The tectonostratigraphy and structure of the eastern Nepal Himalaya. *Tectonics, 11*, 925–943.

Schelling, D., & Arita, K. (1991). Thrust tectonics, central shortening, and the structure of the far-eastern Nepal Himalaya. *Tectonics, 10*, 851–862.

Searle, M. P., Law, R. D., Godin, L., Larson, K., Streule, M. J., Cottle, J. M., et al. (2008). Defining the Himalayan Main Central Thrust in Nepal. *Journal of Geological Society of London, 165*, 523–534.

Searle, M. P., Simpson, R. L., Law, R. D., Parrish, R. R., & Waters, D. J. (2003). The structural geometry, metamorphic and magmatic evolution of the Everest massif, High Himalaya of Nepal-South Tibet. *Journal of Geological Society of London, 160*, 345–366.

Simpson, R. L., Parrish, R. R., Searle, M. P., & Waters, D. J. (2000). Two episodes of monazite crystallization during metamorphism and crustal melting in the Everest region of the Nepalese Himalaya. *Geology, 28*, 403–406.

Tajcmanová, L., Connolly, J. A. D., & Cesare, B. (2009). A thermodynamic model for titanium and ferric iron solution in biotite. *Journal of Metamorphic Geology, 27*, 153–164.

Thakur, S. S., & Patel, S. C. (2012). Mafic and pelitic xenoliths in the Kinnaur Kailash Granite, Baspa river valley, NW Himalaya: evidence of pre-Himalayan granulite metamorphism followed by cooling event. *Journal of Asian Earth Sciences, 56*, 105–117.

Tobgay, T., Long, S., McQuarrie, N., Ducea, M. N., & Gehels, C. (2010). Using isotopic and chronologic data to fingerprint strata: challenges and benefits of variable sources to tectonic interpretations, the Paro Formation, Bhutan Himalaya. *Tectonics, 29*, TC6023. doi:10.1029/2009TC002637.

Vannay, J. C., & Grasemann, B. (2001). Himalayan inverted metamorphism and syn-convergence extension a consequence of a general shear extrusion. *Geological Magazine, 138*, 253–276.

Vannay, J. C., & Hodges, K. V. (1996). Tectonometamorphic evolution of the Himalayan metamorphic core between the Annapurna and Dhaulagiri, central Nepal. *Journal of Metamorphic Geology, 14*, 635–656.

Viskupic, K., Hodges, K. V., & Bowring, S. A. (2005). Timescales of melt generation and the thermal evolution of the Himalayan metamorphic core, Everest region, eastern Nepal. *Contributions to Mineralogy and Petrology, 149*, 1–21.

Wang, J. M., Zhang, J. J., & Wang, X. X. (2013). Structural kinematics, metamorphic P–T profiles and zircon geochronology across the Greater Himalayan crystalline complex in south-

central Tibet: implication for a revised channel flow. *Journal of Metamorphic Geology, 31*, 609–628. doi:10.1111/jmg.12036.

White, R. W., Powell, R., Holland, T. J. B., & Worley, B. A. (2000). The effect of TiO_2 and Fe_2O_3 on metapelitic assemblages at green schist and amphibolite facies conditions: mineral equilibria calculations in the system K_2O–FeO–MgO–Al_2O_3–SiO_2–H_2O–TiO_2–Fe_2O_3. *Journal of Metamorphic Geology, 18*, 497–511.

Zenk, M., & Schulz, B. (2004). Zoned Ca-amphiboles and related P–T evolution in metabasites from the classical Barrovian metamorphic zones in Scotland. *Mineralogical Magazine, 68*, 769–786.